Journal of Southeast University (English Edition) Vol. 24, No. 4, pp. 492 – 497 Dec. 2008 ISSN 1003—7985

Joint torque-based Cartesian impedance control with friction compensations

Liu Yechao Jin Minghe Liu Hong

(Robotics Institute, Harbin Institute of Technology, Harbin 150001, China)

Abstract: In order to investigate the joint torque-based Cartesian impedance control strategies and the influence of compensations for friction, an experimental study on the identification of friction parameters, friction compensation and the Cartesian impedance control are developed for the harmonic drive robot, by using the sensors available in the joint itself. Different from the conventional Cartesian impedance control schemes which are mostly based on the robot end force/torque information, five joint torque-based Cartesian impedance control schemes are considered, including the force-based schemes in Cartesian/joint space, the position-based schemes in Cartesian/joint space and the stiffness control. Four of them are verified by corresponding experiments with/without friction compensations. By comparison, it is found that the force-based impedance control strategy is more suitable than the position-based one for the robot based on joint torque feedback and the friction has even a positive effect on Cartesian impedance control stability.

Key words: Cartesian impedance control; harmonic drive; friction identification; friction compensation; joint torque

Harmonic drive transmissions are widely used in many precision positioning applications. However, some factors such as friction, joint flexibility, nonlinearity and hysteresis degrade system performance. A substantial body of previous research exists in the area of modeling harmonic drive friction[1-4]. Although these research efforts have provided significant insight into the physical phenomena that characterize harmonic drive behavior, all their experimental work has been performed on custom-designed, elaborate testbeds that allow direct measurement of many important system parameters such as compliance and kinematic transmission error. Our work is distinct from these previous works in that the joint friction caused by harmonic drive can be identified and compensated for only by using the sensors which are available in the joint itself, such as the input motor current, the joint torque sensor and the motor shaft encoder.

Even though compensating for friction, controlling the interaction of a robot manipulator with the environment is still a very complicated problem. Impedance control[5-7] has been widely adopted by many researchers. But most control schemes adopted in the industrial robot need a force sensor at the robot end to detect the interaction force, which are practically impossible to detect the collision occurred on the manipulator structure. Albu-Schäffer et al.[8-13] gave many experimental investigations on Cartesian impedance control for the DLR-light-weight-arms with/without an end force/torque sensor and proved asymptotical stability based on passivity theory. However, few comparative results were analyzed in their experiments. Our distinct contribution from these previous works is that in this paper we not only present different impedance control schemes but also identify the friction parameters and compare these different strategies in experiments with/without friction compensations on our flexible joint manipulator which has only a joint torque sensor in each joint and no end force/torque sensor.

1 Cartesian Impedance Control Methods

In this section we summarize some control methods, which can be used to obtain the desired compliant robot behavior in Cartesian space for an end-force sensor-less robot. Because there is no force sensor in the robot end, if necessary, the Cartesian force at the robot end is computed according to the joint torque which is measured from the joint torque sensor directly. As we know, the aim of the Cartesian impedance controller is to establish a mass-damper-spring relationship between the Cartesian position $\Delta \boldsymbol{x}$ and the Cartesian force $\boldsymbol{F}$:

$$\boldsymbol{F} = \boldsymbol{M}_{\mathrm{k}} \Delta \ddot{\boldsymbol{x}} + \boldsymbol{D}_{\mathrm{k}} \Delta \dot{\boldsymbol{x}} + \boldsymbol{K}_{\mathrm{k}} \Delta \boldsymbol{x} \qquad \Delta \boldsymbol{x} = \boldsymbol{x}_{\mathrm{f}} - \boldsymbol{x} \qquad (1)$$

where $\boldsymbol{M}_{\mathrm{k}}$, $\boldsymbol{D}_{\mathrm{k}}$, $\boldsymbol{K}_{\mathrm{k}}$ and $\boldsymbol{x}_{\mathrm{f}}$ are positive definite matrices representing the virtual inertia, the damping, the stiffness of the system and the desired reference Cartesian position, respectively. In the following, we will focus on five control strategies for the impedance control.

1.1 Force-based scheme in Cartesian space for impedance control (FB-CS-IC)

As shown in Fig. 1, the control algorithm is realized in Cartesian space in the FB-CS-IC structure. The impedance control directly uses Eq. (1), in which the actual Cartesian position $\boldsymbol{x}$ is computed from the joint position $\boldsymbol{q}$ using forward kinematics. $\boldsymbol{G}_{\mathrm{c}}(\boldsymbol{f})$ represents the Cartesian force controller (e.g., PI controller), which is in charge of regulating the tracking error between the impedance force $\boldsymbol{F}_{\mathrm{d}}$ and the actual force $\boldsymbol{F}$ computed according to the joint torque. Using the transposed Jacobian $\boldsymbol{J}^{\mathrm{T}}(\boldsymbol{q})$, the control result $\boldsymbol{U}_{\mathrm{f}}$ is transformed into the motor torque command with nonlinearity compensations, such as friction and gravity compensation.

Received 2007-12-12.

Biographies: Liu Yechao (1980—), male, graduate; Liu Hong (corresponding author), male, doctor, professor, dlrhitlab@yahoo.com.cn.

Foundation items: The National Natural Science Foundation of China (No. 60675045), the National High Technology Research and Development Program of China (863 Program) (No. 2006AA04Z255).

Citation: Liu Yechao, Jin Minghe, Liu Hong. Joint torque-based Cartesian impedance control with friction compensations[J]. Journal of Southeast University (English Edition), 2008, 24(4): 492 – 497.

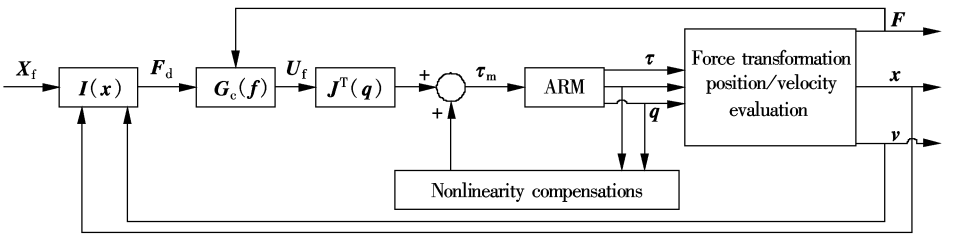

Fig. 1 FB-CS-IC architecture

1.2 Force-based scheme in joint space for impedance control (FB-JS-IC)

This control strategy is similar to the former, as shown in Fig. 2. The remarkable difference is that in this control structure it is not necessary to compute the Cartesian force $\boldsymbol{F}$, because in the control algorithm only joint torque $\boldsymbol{\tau}$ is used. The Cartesian force $\boldsymbol{F}_d$ computed from Eq. (1) is transformed into the desired joint torques directly. The joint torque controller $\boldsymbol{G}_c(\boldsymbol{\tau})$ (e. g., the PD controller in Ref. [9] can be used) generates the motor torque command with the nonlinearity compensations.

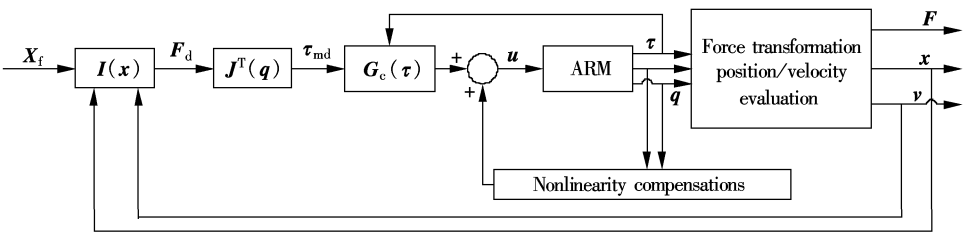

Fig. 2 FB-JS-IC architecture

1.3 Position-based scheme in Cartesian space for impedance control (PB-CS-IC)

The third control structure is the position-based scheme in Cartesian space, which means that a high-gain position controller can be adopted in Cartesian space to compensate for some nonlinear effects, as shown in Fig. 3. The end Cartesian force $\boldsymbol{F}$ can be computed from the joint torque, just as mentioned in the above. $\boldsymbol{H}(f)$ represents the second-order impedance filter, whose parameters are the same as those of Eq. (1). Hence, the desired Cartesian position $\boldsymbol{x}_d$ can be computed by

$$\boldsymbol{x}_d = \boldsymbol{x}_f - \frac{f}{\boldsymbol{M}_k s^2 + \boldsymbol{D}_k s + \boldsymbol{K}_k} \tag{2}$$

Using the Cartesian position controller(e. g. the PD controller) $\boldsymbol{G}_c(\boldsymbol{x})$ and $\boldsymbol{J}^T(\boldsymbol{q})$, the motor torque command can be computed just as shown in Fig. 3.

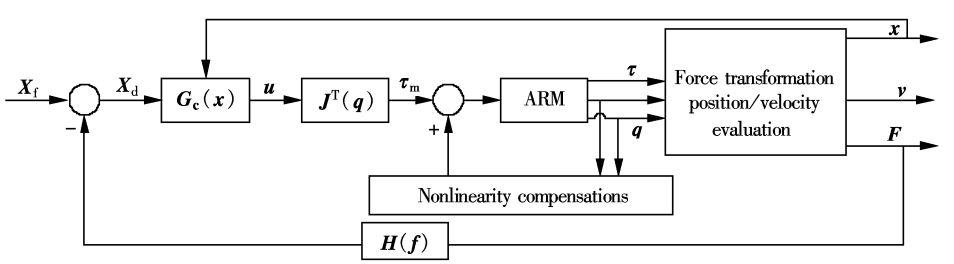

Fig. 3 PB-CS-IC architecture

1.4 Position-based scheme in joint space for impedance control (PB-JS-IC)

As the high-gain joint position controller can compensate for the friction in the joints, another control architecture is presented (see Fig. 4). There are two obvious differences from Fig. 3. One is that the position controller $\boldsymbol{G}_c(\boldsymbol{q})$ is for the joint position, not for the Cartesian position; the other is that in this control algorithm inverse kinematics is nece-

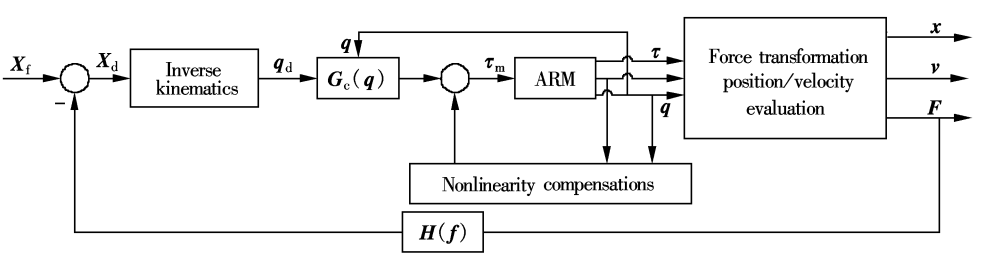

Fig. 4 PB-JS-IC architecture

ssary, which is distinct from the previous three control methods. Because the bandwidth of the Cartesian control loop approaches the joint bandwidth by using the high-gain controller, stability problems will appear for desired low stiffness and damping for this control strategy. This problem is even more noticeable for flexible joint robots, since, in that case, the bandwidth of joint control is more critical.

1.5 Stiffness control

Since the mapping relationship between Cartesian space and joint space can be deduced according to the robot equation, this leads to the idea of converting the desired Cartesian impedance parameters to corresponding parameters for the joint[13-14]. But it is necessary to point out that the mapping as well as the joint impedance parameters $\{\boldsymbol{M}_j, \boldsymbol{D}_j, \boldsymbol{K}_j\}$ has only a local meaning.

$$\boldsymbol{M}_j = \frac{\partial \boldsymbol{\tau}}{\partial \ddot{\boldsymbol{q}}^T} = \frac{\partial(\boldsymbol{J}^T(\boldsymbol{q})\boldsymbol{M}_k \Delta \ddot{\boldsymbol{x}})}{\partial \ddot{\boldsymbol{q}}^T} = \boldsymbol{J}^T(\boldsymbol{q})\boldsymbol{M}_k \boldsymbol{J}(\boldsymbol{q}) \tag{3}$$

$$\boldsymbol{D}_j = \frac{\partial \boldsymbol{\tau}}{\partial \dot{\boldsymbol{q}}^T} = \frac{\partial(\boldsymbol{J}^T(\boldsymbol{q})\boldsymbol{D}_k \Delta \dot{\boldsymbol{x}})}{\partial \dot{\boldsymbol{q}}^T} = \boldsymbol{J}^T(\boldsymbol{q})\boldsymbol{D}_k \boldsymbol{J}(\boldsymbol{q}) \tag{4}$$

$$\boldsymbol{K}_j = \frac{\partial \boldsymbol{\tau}}{\partial \boldsymbol{q}^T} = \frac{\partial(\boldsymbol{J}^T(\boldsymbol{q})\boldsymbol{K}_k \Delta \boldsymbol{x})}{\partial \boldsymbol{q}^T} = \boldsymbol{J}^T(\boldsymbol{q})\boldsymbol{K}_k \boldsymbol{J}(\boldsymbol{q}) + \frac{\partial \boldsymbol{J}(\boldsymbol{q})}{\partial \boldsymbol{q}^T}\boldsymbol{K}_k \Delta \boldsymbol{x} \tag{5}$$

Once the joint impedance parameters are computed by Eqs. (3), (4) and (5), the joint controllers can be designed.

Five control structures are summarized according to the previous research in this section. There are still some remarks to be noted:

1) Owing to the nonlinearities such as joint frictions, the computed Cartesian force $\boldsymbol{F}$ ($\boldsymbol{F} = \boldsymbol{J}^{-T}\boldsymbol{\tau}$) may be not good. In order to eliminate the effects of noise, some filters for force signals are necessary, which is not mentioned in this part.

2) When the manipulator executes some tasks, the force applied by the robot may be decomposed into motion-inducing and internal forces. But in this section, we suppose that the end force of the robot is only an internal force, which is completely transformed into a joint torque by the transposed Jacobian $\boldsymbol{J}^T(\boldsymbol{q})$, and the force decomposition is not referred to.

3) The control structures mentioned above are only considered in ordinary cases. Some special behaviors such as singular configuration and redundancy robots are not discussed in this section.

2 Friction Identification for Harmonic Drive Joint

There are many approaches about friction identification in harmonic drives[1, 15-16]. To describe velocity-dependent friction, we carry out high-gain closed-loop experiments where a PD position controller is used in order to achieve good velocity tracking even at very low velocities. Each joint is commanded to move at a constant velocity and the mean torque required to maintain the velocity is regarded as the friction for that velocity. In order to investigate the friction model accurately as soon as possible, data for joint velocities between 0.5 and 30 (°)/s are collected, which are recorded in different intervals with 1 (°)/s increments between 1 and 6 (°)/s, 2 (°)/s increments between 6 and 20 (°)/s, 5 (°)/s increments between 20 and 30 (°)/s, respectively. Three trials are performed for each velocity in both the positive and negative directions, for a total of 96 measurements per joint. After collecting data for all four joints, we fit three different friction models using the Matlab toolbox, that is, 1) the kinetic plus viscous friction model, 2) the cubic polynomial model, and 3) the Stribeck curve model. The analysis results are shown in Tab. 1 and comparisons are made for different models.

Tab. 1 Different models for friction and their comparisons

Joint	Viscous model			Cubic model			Stribeck model		
	Model DOF	SSE	RMSE	Model DOF	SSE	RMSE	Model DOF	SSE	RMSE
1	2	20.62	1.214	4	3.059	0.504 9	4	3.101	0.508 4
2	2	51.55	1.919	4	38.630	1.794 0	4	39.110	1.805 0
3	2	33.55	1.548	4	3.155	0.512 7	4	5.437	0.673 1
4	2	96.53	2.383	4	5.351	0.597 3	4	5.916	0.628 0

Through the comparisons of different models, we find that the Stribeck model provides a reasonable and intrinsic description for harmonic driving friction. It is worth noting that the residual variance for the cubic model presented by Tuttle[2] is smaller than that for the Stribeck model for the robot's joints. But we find that the differences are remarkable between models fit by whole data and by partial data when using the cubic model. For example, we have acquired 16 experimental data to describe the relationship between friction torque and joint velocity, and find that the cubic model parameters fit by the first 14 data are obviously distinct from those fit by the whole 16 data. The cubic model is invalid beyond the velocity zone where the identification experiments are not executed. It seems that this model just makes the fit curve "look" good, but does not expose the intrinsic rule of the harmonic friction. This inconsistent phenomenon is not so remarkable in the Stribeck model. As shown in Fig. 5, curve 1 is the cubic curve approximation fit by the first 14 data and curve 2 is that fit by the whole 16 data; curve 3 is the Stribeck curve approximation fit by the first 14 data and curve 4 is that fit by the whole 16 data. It is clear that the Stribeck model is better than the cubic model in modeling the harmonic friction. So, in our experiments we adopt the Stribeck model as the friction model of the harmonic drive. For convenience, the expression for this model is given by

$$T_{vf}(v) = a\exp(-bv) + cv + d \tag{6}$$

where a, b, c, d are parameters to be identified for the model. Tab. 2 gives the Stribeck coefficients for all joints.

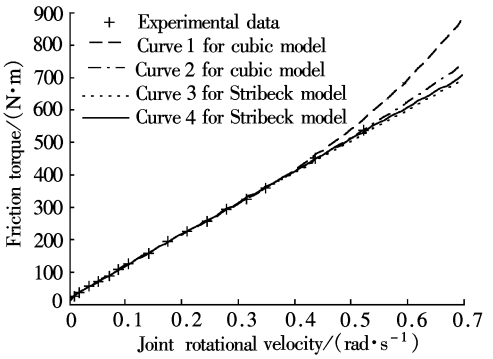

Fig. 5 Curves for different friction models

Tab. 2 Coefficients for Stribeck curve describing friction behavior for all joints in both positive and negative directions

Direction	Joint	Coefficients			
		a	*b*	*c*	*d*
Positive direction	1	−41.97	1.88	941.3	62.72
	2	−9.63	99.24	978.5	19.06
	3	−8.01	14.58	235.5	12.39
	4	−21.05	3.76	215.6	26.84
Negative direction	1	10.87	−5.65	961.7	−31.78
	2	5.91	−51.49	972.2	−20.27
	3	7.69	−17.58	236.5	−11.71
	4	19.15	−4.39	218.1	−24.40

3 Experiments

To demonstrate the general validity of the proposed control architectures, four experiments using the first four control structures except the stiffness control mentioned in section 1 were executed on our robot. The experiments were related to typical application areas for impedance control: contact with unknown, stiff but passive environments. During these experiments, we compare the control results and conclude their advantages and disadvantages, respectively.

The experiment setup is shown in Fig. 6. The manipulator is commanded to move in the vertical (z) direction. After the impact with an aluminium surface, the force at the robot end increases proportionally to the position error. The commanded stiff values for these experiments are 5 000 N/m, 5 000 N/m and 500 N/m in x, y and z directions, respectively. The stiffness in z direction is smaller in order to have a reasonable steady-state force. The plots of position and force in z direction are given in the following using the different control strategies, respectively. For comparison, comparative experiments with/without friction compensation are executed (see Fig. 7 and Fig. 8). Among them, the first four figures are the experimental results using the force-based control strategy; that is, (a) and (b) are the results obtained using the FB-CS-IC strategy, and (c) and (d) are the results obtained using the FB-JS-IC strategy, respectively. At the same time, for comparison, the following four figures show the control results using position based control schemes, where (e) and (f) are the results obtained using the PB-CS-IC strategy, and (g) and (h) are the results obtained using the PB-JS-IC strategy.

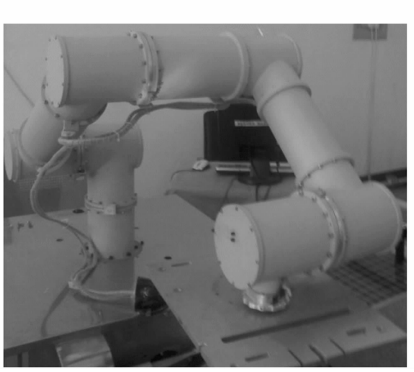

Fig. 6 The setup for the impact experiment

From the comparison experiments, some remarks about advantages and disadvantages of the presented strategies are given in the following:

1) Owing to the integrator control, the FB-CS-IC strategy can maintain a small steady error. Even under the condition of the small desired Cartesian impedance stiffness, the system is also stable. But unfortunately, when the robot impacts with the stiff environment, the force will vibrate slightly, which will degrade the system's stability(see Figs. 7(a) and (b)). If there is no friction compensation, the stability may be improved (see Figs. 8(a) and (b)), but the tracking performance will degrade.

2) The FB-JS-IC strategy provides a good trade-off between the system's performance and stability. Due to the PD controller's adoption in joint torque control, the system's damping can be increased and the passivity properties can be maintained, which makes the system stable even under the condition of the small desired Cartesian impedance stiffness. When the robot impacts with the stiff environment, good performances can be achieved using this strategy not only in the transition state but in the steady state no matter whether friction compensations are in or not(see Figs. 7(c) and (d), Figs. 8(c) and (d)).

3) Though the PB-CS-IC and the PB-JS-IC strategies can guarantee good tracking performances in large Cartesian impedance stiffness with friction compensation(see Figs. 7 (e) and (g)), interactions with the stiff environment are often unstable when using the same control parameters (see Figs. 8(f) and (h)). If stability is assured under the same conditions, the gains in the position loop must be decreased greatly, which will affect the performance badly. Even without friction compensation, there are two obvious shortcomings: bad tracking performance for PB-CS-IC(see Figs. 8 (e) and (f)) and instability for PB-JS-IC(see Figs. 8(g) and (h)).

4) Friction compensation can improve the system's tracking performance and compliance ability, but the stability of the system will be affected negatively (see Figs. 7 and 8).

Hence, it can be recognized that the force-based impedance strategies are better than the position-based impedance strategies for the end-force sensor-less robot with a harmonic drive transmission. Interestingly, for the force-based strategies, the friction has even a positive effect on Cartesian impedance control stability[7], which is also found in our experiments. However, performance degradation is introduced by tracking errors.

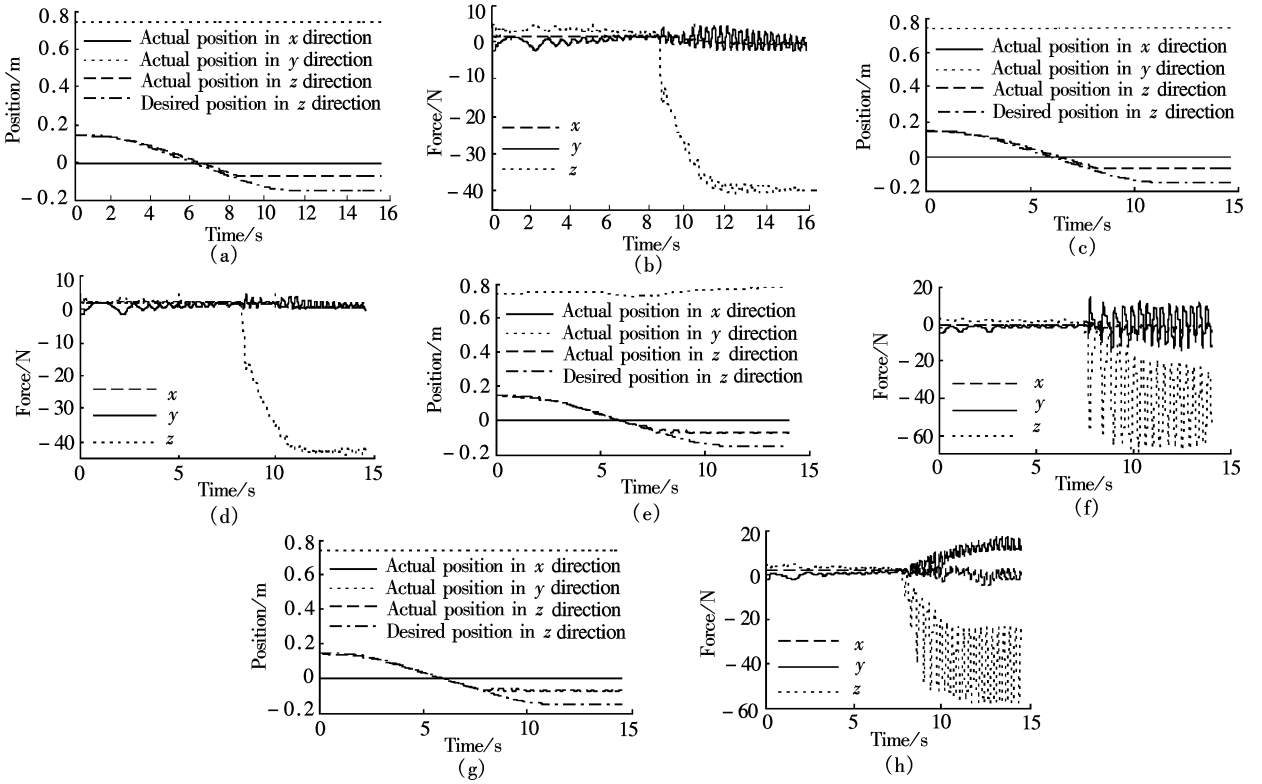

Fig. 7 Position and force using different control schemes with friction compensation. (a) Position displacements using the FB-CS-IC strategy; (b) Forces using the FB-CS-IC strategy; (c) Position displacements using the FB-JS-IC strategy; (d) Forces using the FB-JS-IC strategy; (e) Position displacements using the PB-CS-IC strategy; (f) Forces using the PB-CS-IC strategy; (g) Position displacements using the PB-JS-IC strategy; (h) Forces using the PB-JS-IC strategy

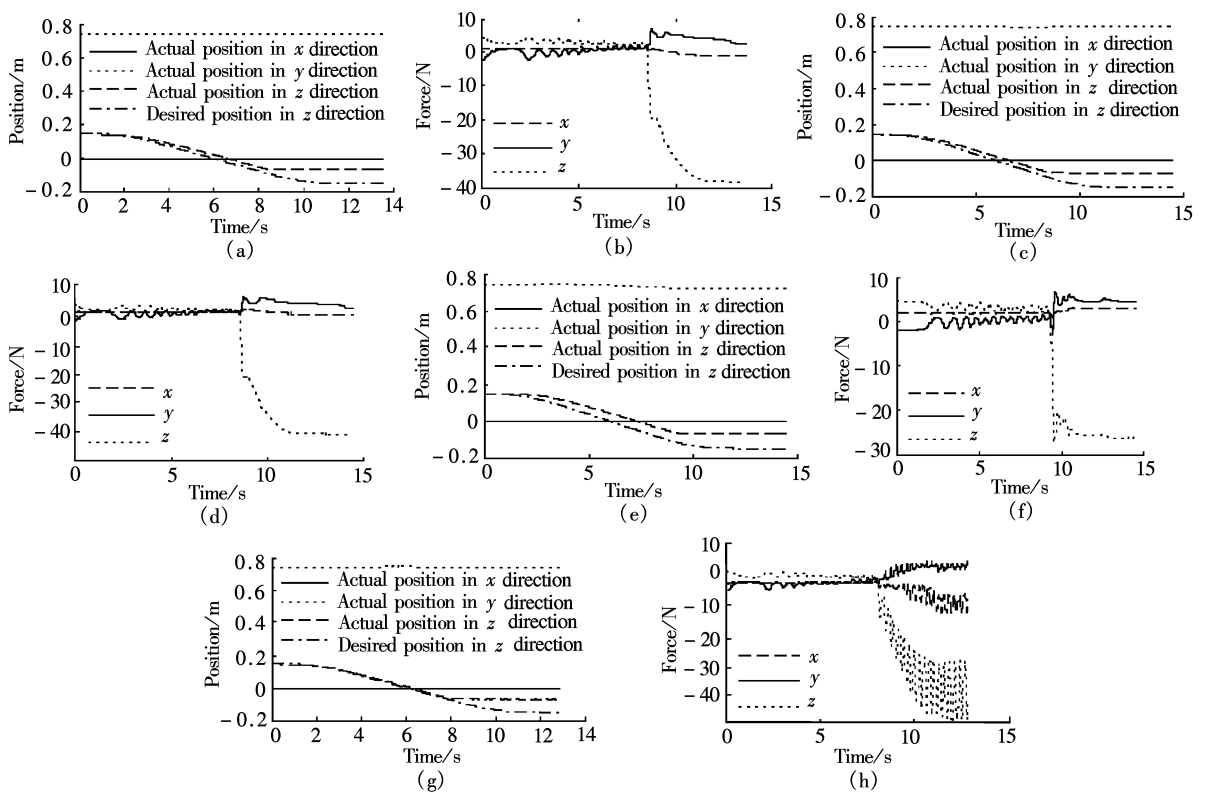

Fig. 8 Position and force using different control schemes without friction compensation. (a) Position displacements using the FB-CS-IC strategy; (b) Forces using the FB-CS-IC strategy; (c) Position displacements using the FB-JS-IC strategy; (d) Forces using the FB-JS-IC strategy; (e) Position displacements using the PB-CS-IC strategy; (f) Forces using the PB-CS-IC strategy; (g) Position displacements using the PB-JS-IC strategy; (h) Forces using the PB-JS-IC strategy

4 Conclusion

A number of Cartesian impedance control schemes are experimentally tested for the end-force sensor less robot with harmonic drive friction compensation. The performance of the schemes using the force-based scheme strategies is shown to be generally superior to that of the schemes using the position-based strategies for the end-force sensor less robot. Among all the various schemes, the force-based scheme in joint space for impedance control gives the most encouraging results not only with large impedance stiffness but with small impedance stiffness. Even in the case of interaction with the stiff environment, good capabilities can also be achieved. This is quite promising to foresee real applications of the control strategy on some end-force sensor less robots with harmonic drive transmissions.

Only the translational impedance parameters are considered in our experiments. Future research efforts will be devoted to extending the work to rotational impedance tasks and giving theoretical explanations for the experimental control strategy.

References

[1] Gandhi P S, Ghorbel F H, Dabney J. Modeling, identification, and compensation of friction in harmonic drives[C]// *Proc of IEEE the* 41*st Conference on Decision and Control*. Las Vegas, 2002: 160 - 166.

[2] Tuttle T D, Seering W P. A nonlinear model of a harmonic drive gear transmission[J]. *IEEE Trans Robot Automat*, 1996, **12**(3): 368 - 374.

[3] Kircanski N M, Goldenberg A A. An experimental study of nonlinear stiffness, hysteresis, and friction effects in robot joints with harmonic drives and torque sensors[J]. *Int J Robot Res*, 1997, **16**(2): 214 - 239.

[4] Taghirad H D. On the modeling and identification of harmonic drive systems, Technical Report CIM-TR-97-02 [R]. McGill University, 1997.

[5] Bonitz R G, Hisa T C. Internal force-based impedance control for cooperating manipulators[J]. *IEEE Trans Robot Automat*, 1996, **12**(1): 78 - 89.

[6] Schneider S A, Cannon R H Jr. Object impedance control for cooperative manipulation: theory and experimental results [J]. *IEEE Trans Robot Automat*, 1992, **8**(3): 383 - 394.

[7] Gonzalez J J, Widmann G R. A force commanded impedance control scheme for robots with hard nonlinearities[J]. *IEEE Trans Control System Tech*, 1995, **3**(4): 398 - 408.

[8] Albu-Schäffer A, Ott C, Freses U, et al. Cartesian impedance control of redundant robots: recent results with the DLR-light-weight-arms[C]//*Proceedings of the IEEE Int Conference on Robotics and Automation*. Taipei, China, 2003: 14 - 19.

[9] Albu-Schäffer A, Ott C, Hirzinger G. Passivity based Cartesian impedance control for flexible joint manipulators[C]// 6*th IFAC Symposium on Nonlinear Control Systems*. Stuttgart, 2004: 1175 - 1180.

[10] Ott C, Albu-Schäffer A, Kugiy A, et al. A passivity based Cartesian impedance controller for flexible joint robots—part Ⅰ: torque feedback and gravity compensation[C]// *Proceedings of the IEEE Int Conference on Robotics and Automation*. New Orleans, 2004: 2659 - 2665.

[11] Albu-Schäffer A, Ott C, Hirzinger G. A passivity based Cartesian impedance controller for flexible joint robots—part Ⅱ: full state feedback, impedance design and experiments [C]//*Proceedings of the IEEE Int Conference on Robotics and Automation*. New Orleans, 2004: 2666 - 2672.

[12] Albu-Schäffer A, Ott C, Hirzinger G. A unified passivity based control framework for position, torque and impedance control of flexible joint robots[C]//*Int Symposium on Robotics Research*. San Francisco, 2005: 5 - 21.

[13] Albu-Schäffer A, Hirzinger G. Cartesian impedance control techniques for torque controlled light-weight robots[C]// *Proceedings of Int Conference on Robotics and Automation*. Washington DC, 2002: 657 - 663.

[14] Salisbury J K. Active stiffness control of a manipulator in Cartesian coordinates[C]//*Proceedings of the* 19*th IEEE Conference on Decision and Control*. Alburquerque, NM, 1980: 83 - 88.

[15] Kennedy C W, Desai J P. Modeling and control of the Mitsubishi PA-10 robot arm harmonic drive system[J]. *IEEE/ASME Trans Mechatronics*, 2005, **10**(3): 263 - 274.

[16] Armstrong-Helouvry B. *Control of machines with friction* [M]. Norwell, MA: Kluwer, 1991: 97 - 103.

摩擦补偿下基于关节力矩的笛卡尔阻抗控制

刘业超　金明河　刘　宏

（哈尔滨工业大学机器人研究所，哈尔滨 150001）

摘要：为了研究基于关节力矩信息的笛卡尔阻抗控制策略及摩擦补偿的影响，利用关节本身具有的传感器，进行了辨识谐波驱动摩擦参数、摩擦补偿和笛卡尔阻抗控制的实验研究. 与传统的基于机器人末端力/力矩信息的笛卡尔阻抗控制方案不同，考虑了 5 种基于关节力矩的笛卡尔阻抗控制方案，包括笛卡尔空间/关节空间基于力的、笛卡尔空间/关节空间基于位置的方案和刚度控制. 其中，前 4 种方案分别在有/无摩擦补偿的条件下进行了相应的实验验证. 实验比较结果表明：对于基于关节力矩信息来实现笛卡尔阻抗控制的机器人，基于力的阻抗控制策略比基于位置的策略更适合，并且摩擦对这类笛卡尔阻抗控制的稳定性有积极影响.

关键词：笛卡尔阻抗控制；谐波驱动；摩擦辨识；摩擦补偿；关节力矩

中图分类号：TP242